Analysis of structure and bonding strength of AlTiN coatings by cathodic ion plating

Kong Dejun · Guo Haoyuan

Abstract AlTiN coating was prepared on the surface of YT14 hard alloy cutter by cathodic arc ion plating, and the surface-interface morphologies, line scans of the interface elements and valence state of chemical elements were analyzed with field emission scanning electron microscopy, energy dispersive spectrometer and X-ray photoelectron spectroscopy, respectively, and bonding strength of the coating was measured with scratching tester. The results show that the elements of Al and N mainly exist in the AlTiN coating with an AlN and AlTiN hard phase, and (the) Ti element mainly exists in the coating with a TiN hard phase, which improve wear resistance of AlTiN coating. The elements of Al, Ti and N are diffused at the coating interface, in which part of Ti atoms are replaced by Al atoms at the TiN lattice, still keep face-centered cubic structure of TiN coating to form metallurgical bonding, and bonding strength of the coating interface measured by scratching tester is 78.75 N, which is beneficial to improving service life of AlTiN coating prepared on the surface of carbide tool cutter.

Keywords Cathode ion plating · Hard alloy cutter · AlTiN coating · XPS analysis · Bonding strength

K. Dejun (✉) · G. Haoyuan
College of Mechanical Engineering, Changzhou University,
Changzhou 213164, People's Republic of China
e-mail: kong-dejun@163.com

K. Dejun
Jiangsu Key Laboratory of Materials Surface Science and
Technology, Changzhou University, Changzhou 213164,
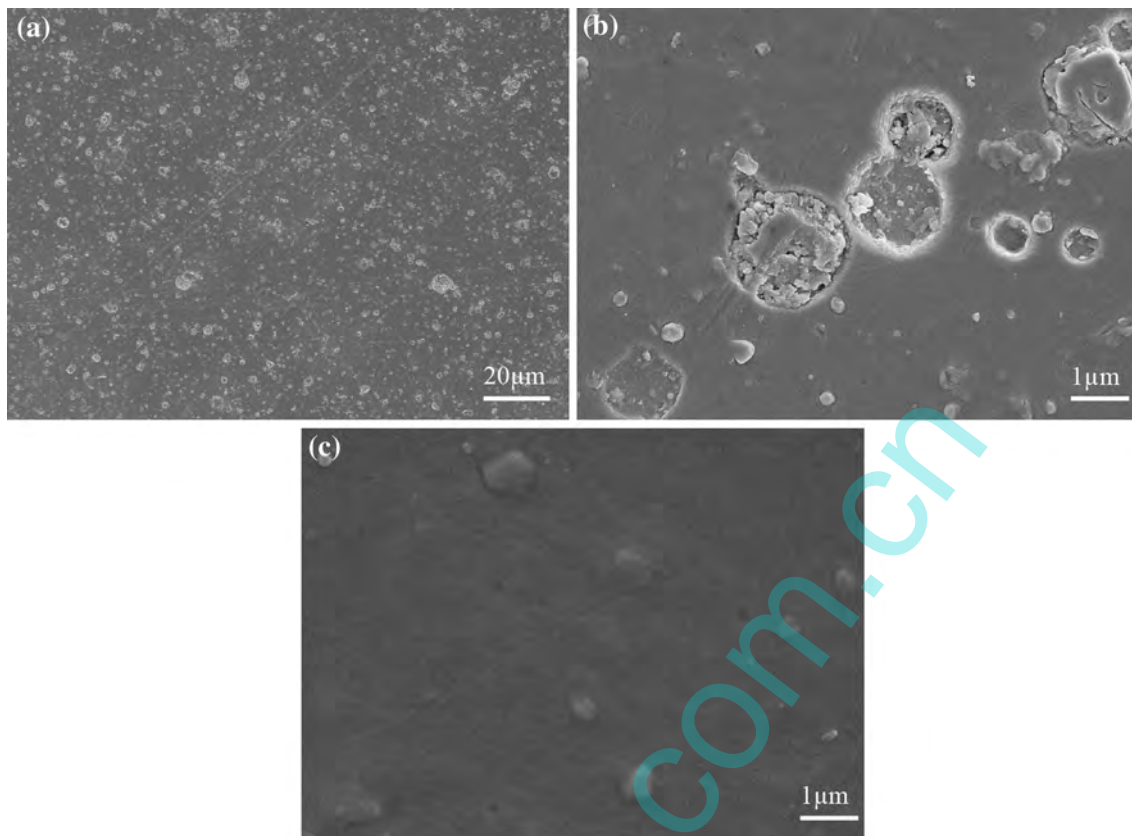People's Republic of China

1 Introduction

Coating technologies not only improve manufacturing efficiency and service life of the cutting tools, but also reduce product costs, which is an important way to increase the tool performances [1, 2]. With the development of surface technologies and hardened processing of the new materials, the higher requirements are put forward on wear resistance, toughness and red hardness of tool coatings [3–5]. Due to brittle, weak binding force, poor oxidation resistance at high temperature, the traditional TiN coatings can hardly meet the cutting requirement of difficult machining materials. As a result, an AlTiN coating is formed by adding Al atom into the TiN coating with chemical stability, hardness and oxidation resistance that has the better mechanical properties than TiC, TiN and TiCN, and may compose multilayer composite coating with other coatings to increase the usage performances of tool coatings further [6–10]. A lot of researches have conducted on AlTiN coating at home and abroad, but little has been reported about the valence state of each element and line scans of interfacial elements of AlTiN coating. AlTiN coating was prepared on the surface of YT14 hard alloy cutter by cathodic arc ion plating in this study, the surface–interface morphologies, line scans of interface elements and valence state of elements were analyzed with field emission scanning electron microscopy (FESEM), energy dispersive spectrometer (EDS) and X-ray photoelectron spectroscopy (XPS), respectively, and bonding strength of the coating was measured with scratching tester, providing an experimental basis for the surface modification of high-speed cutting tools.

Fig. 1 Morphologies and defects of AlTiN coating surface. **a** Low magnification morphology, **b** surface pits **c** surface particles
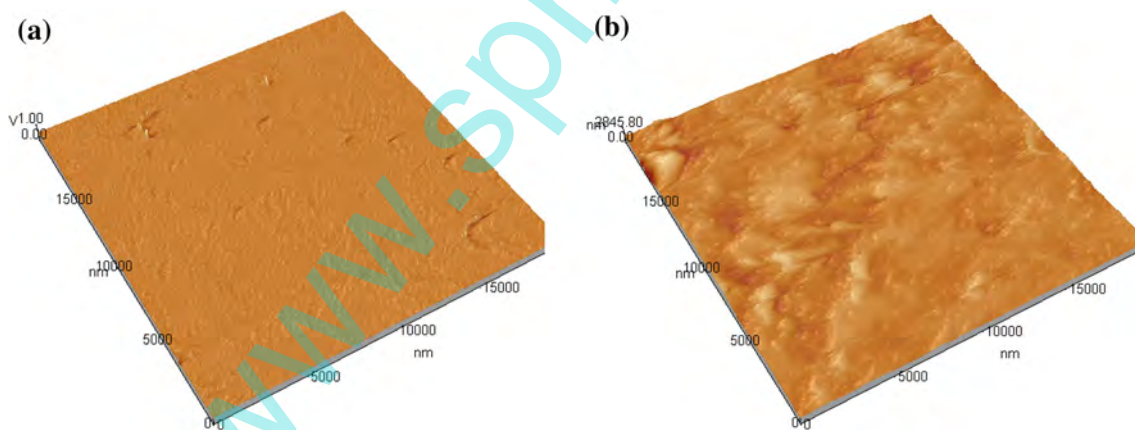

Fig. 2 AFM of substrate and AlTiN coating surfaces. **a** Substrate, **b** AlTiN coating

2 Experimental

The substrate material was YT14 hard alloy cutter with the chemical compositions as follows (mass %): WC 78, TiC 14, Co 8, polished by the sandpapers 80#, 120#, 200#, 600#, 800# and metallographic sandpaper in turn with the surface roughness of 0.1 μm. Before putting the

samples into the vacuum chamber, the samples were cleaned in pure acetone using ultrasonic oscillation for 5–10 min. After rising in pure ethanol, the samples were dried up before being deposited in a PVT coating system. The preparation process shown as follows: (1) The vacuum pumping system with a turbo-molecular pump was used to create a vacuum in the chamber with 5.0×10^{-4}
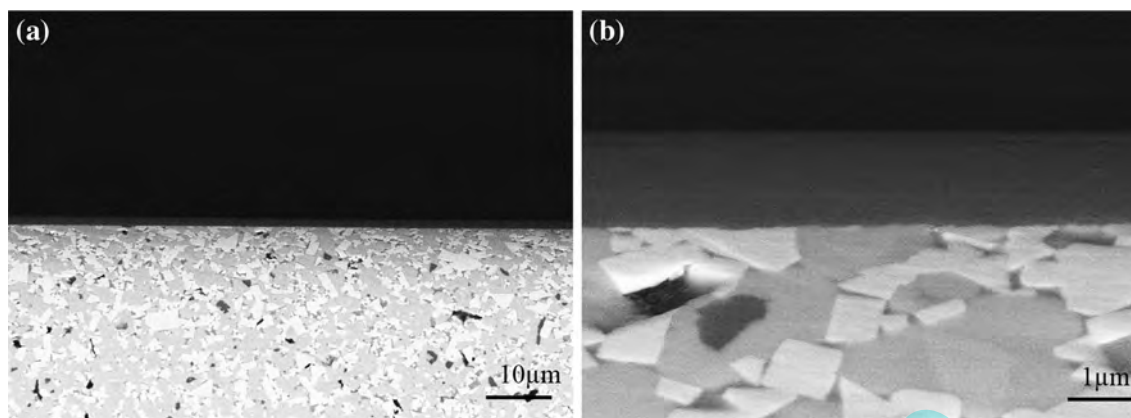
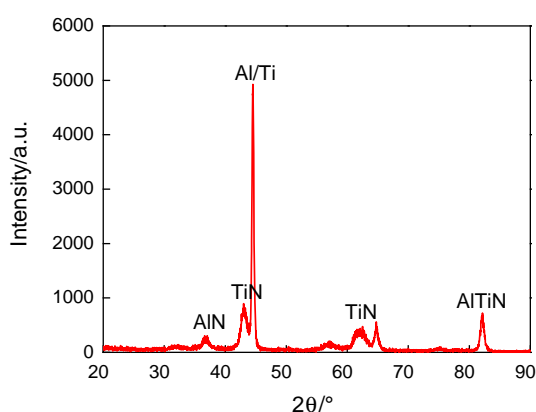**Fig. 3** Interface morphologies of AlTiN coatings. **a** Low magnification, **b** high magnification

Fig. 4 XRD diffraction pattern of AlTiN coatings

Pa, besides the sample surfaces were cleaned and heated by Ar and Ti ion. (2) In order to deposit AlTiN multiple coatings, Ti–Al composite target (atomic ratio = 1:1) was adopted, and the deposition time was held at 120 min for the AlTiN coating. (3) After deposition, inletting N_2 to cool for 15 min. The technological parameters of cathode ion plating: bias power of −100 V, target electric current of 80 A, duty cycle 30 %, gas pressure of 1.2 Pa. The surface–interface morphologies and line scans of interface elements were observed with JSUPRA55 type FESEM and its configured EDS, the surface roughness was measured with a CSPM5500 type AFM (atomic force microscope) and microhardness of the coating was measured by HV-1000 type micro vickers hardness tester with load: 0.3 N and time: 15 s. The valence state of elements was analyzed with a Thermo ESCALAB 250 type XPS, X-ray excitation source: monochrome Al Ka (hv = 1486.6 eV), power of 150 V, X-ray beam spot of 500 μm, energy of 30 eV. Bonding strength of the coating was measured with WS-2005 type scratching tester, the measured method:

acoustic emission, load of 100 N, loading rate of 50 N/min and scratch length of 6 mm.

3 Results and discussion

3.1 Surface–interface morphologies

The surface of AlTiN coating was relatively smooth with compact structures and fine particles, as shown in Fig. 1a, which was because that the Ti and Al target were replaced by Ti–Al composite target in deposition process. As the number of large particles produced by low melting point metal target was much higher than that of high melting point metal target. The melting point of Ti–Al composite target was much higher than that of pure Al in a way, which reduced the large particles generate during the deposition process. At the same time, the increase in nitrogen pressure was also contributed to reduce the particulate pollution of the coating surface, which improved the coating surface roughness in some way [11]. There were some pits during the deposition of low melting point metal, as shown in Fig. 1b, in which the coating growth was an island mode. The growth mechanism was that the evaporation source emitted some atoms with energy gas phase which were adsorbed on the substrate surface, when they migrated to the steps or defects of substrate surface, and the atoms with gas phase stayed here. With the increasing of the atoms and atomic clusters, they collided and combined with each other to form a stable number of large atomic clusters that was the critical nucleus. After forming of the critical nucleus, they captured other atoms and combined with incident vapor atoms to further grow to the small island, as shown in Fig. 1c.

The average surface roughness was 0.00744 nm with AFM, as shown in Fig. 2a, while the average surface
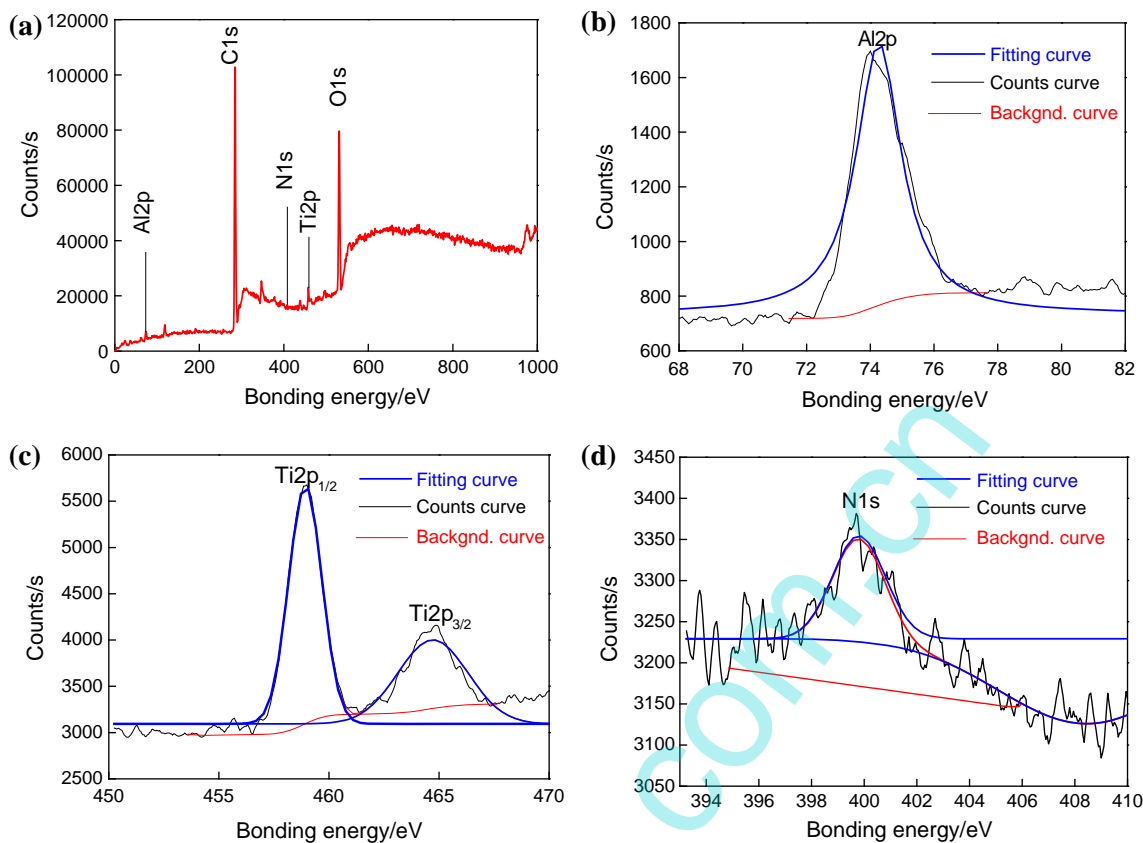
Fig. 5 XPS spectra of AlTiN coating surface. **a** Full spectrum, **b** Al element, **c** Ti element, **d** N element

roughness of AlTiN coating was 98.9 mm, as shown in Fig. 2b.

As shown in Fig. 3a, the thickness of AlTiN coating was about 1.78 μm, which had a good combination and continuous dense with the substrate. The structure of the coating was compact with no coarse columnar grains and holes, as shown in Fig. 3b.

3.2 XRD analysis

The XRD results of the AlTiN coating were shown in Fig. 4. There were Al/Ti, AlN, TiN and AlTiN hard phases existed in the AlTiN coating, appearing a strong Al/Ti diffraction peak at 2θ value of 44.52°. The Ti element mainly existed in the coating with TiN hard phase, which were observed at 2θ value of 43.02° and 63.04°, respectively. The elements of Al and N mainly existed in AlTiN coating with AlN and AlTiN hard phases, and the weak diffraction peaks of AlN and AlTiN hard phase were emerged at 2θ value of 38.1° and 82.22°, respectively. The radius of Ti atom was 0.146 nm, while that of Al atom was 0.143 nm, both of which were not so far. Part of Ti atoms were replaced by Al atoms at TiN lattice to form a crystal structure of AlTiN, and still kept face-centered cubic (FCC) structure of TiN coating during the deposition process. Comparing with reflections of (111) and (200) planes of cubic

TiN observed at 2θ value of 36.7° and 61.9°, respectively, there was a wide phenomenon of AlTiN diffraction peak [12]. When the Al atoms formed a substitutional solid solution at TiN lattice, the forming of crystal surface was changed, and the lattices produced a large distortion and dislocation, which was benefited to improving the hardness of AlTiN phase with 3,000 HV measured by micohardness tester. Because of the limited solubility of Al in TiN phase, the alloy system of AlTiN would be unstable and easily cause the decomposition to form phase separations, as a result, there appeared strong Al/Ti diffraction peak in the AlTiN coating.

3.3 XPS analysis

In order to detect the signals of Al2P, Ti2p, N1s, O1s and C1s, a XPS full spectrum of AlTiN coating was analyzed in the surface depth of 1–3 nm, as shown in Fig. 5a. Besides the characteristic peaks of Al, Ti and N elements in the XPS full spectrum of AlTiN coating, there were still strong peaks of O1s and C1s duo to the coating exposed to the air. Al element was corresponded with two kinds of chemical environment. Binding energy of 74.12 eV was corresponded with AlN phase, whose standard binding energy was 73.8 eV, and binding energy of 74.36 eV was corresponded with a few Al_2O_3, whose standard binding energy

Fig. 6 Line scans of AlTiN coating interface. **a** Al element, **b** Ti element, **c** N element, **d** C element, **e** O element, **f** W element, **g** Co element
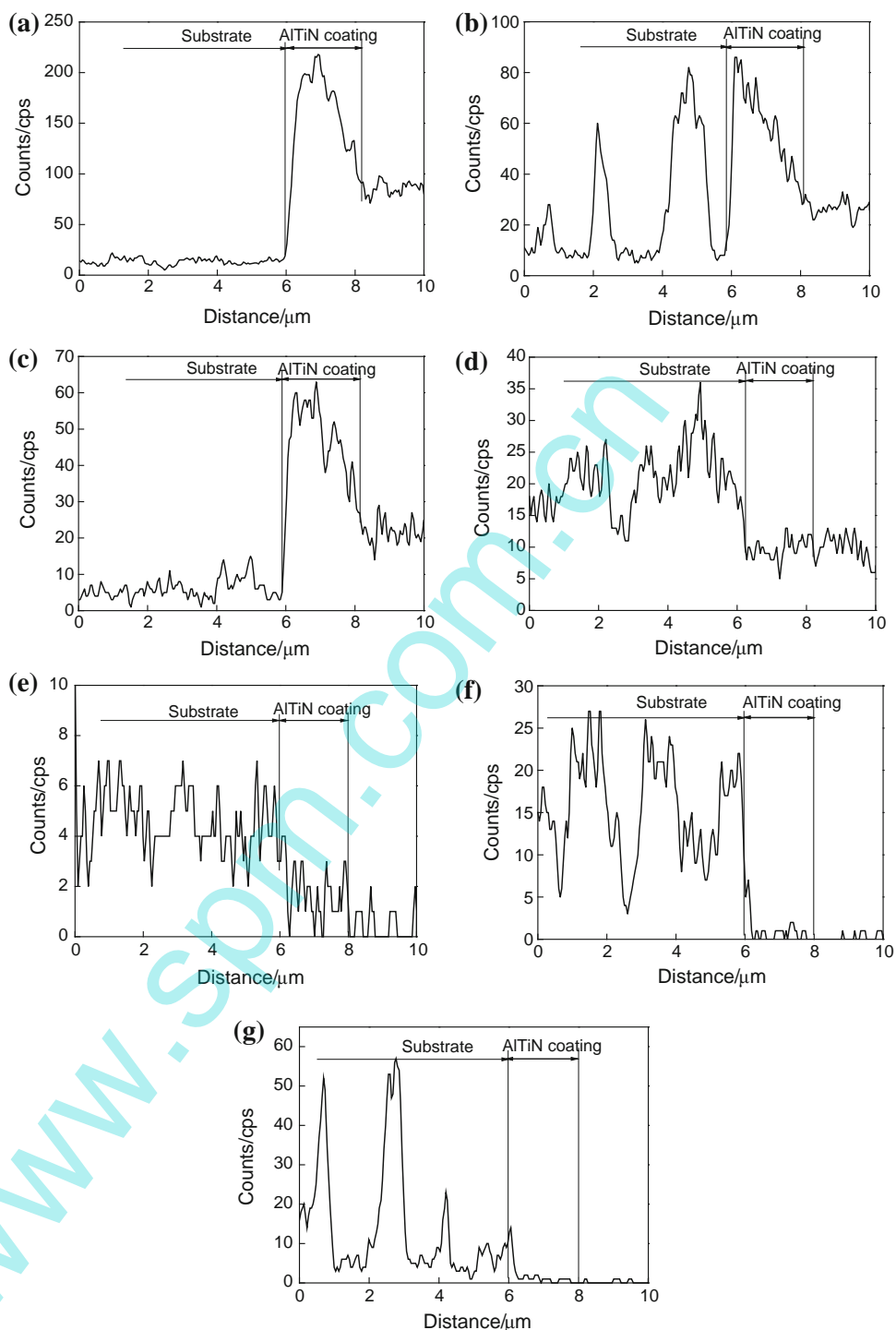
was 74.3 eV, as shown in Fig. 5b. Figure 5c shows that the characteristic peak of Ti was small, and the peak intensity was very weak. There were TiN and TiO$_2$ as considering the chemical environment of Ti elements, the binding energies of TiN and TiO$_2$ had been reported to be 458.90 and 464.85 eV for TiN and TiO$_2$, respectively. Compared with the binding energy of XPS chart, the standard binding energy of Ti element was 454.30 and 460.35 eV,

respectively. The results revealed that the peak value of Ti shifted to the left of 4.60 eV, compared with the binding energies of Ti2p$_{1/2}$ (462.1 eV) and Ti2p$_{3/2}$ (456.80 eV) in AlTiN coating measured by literatures [13]. Therefore, it was inferred that the Ti2p spectrum was corresponded with Ti–N in AlTiN phase. There were two possible situations of AlN phase and N–O key for N element peak, as shown in Fig. 5d, the standard binding energy of AlN was
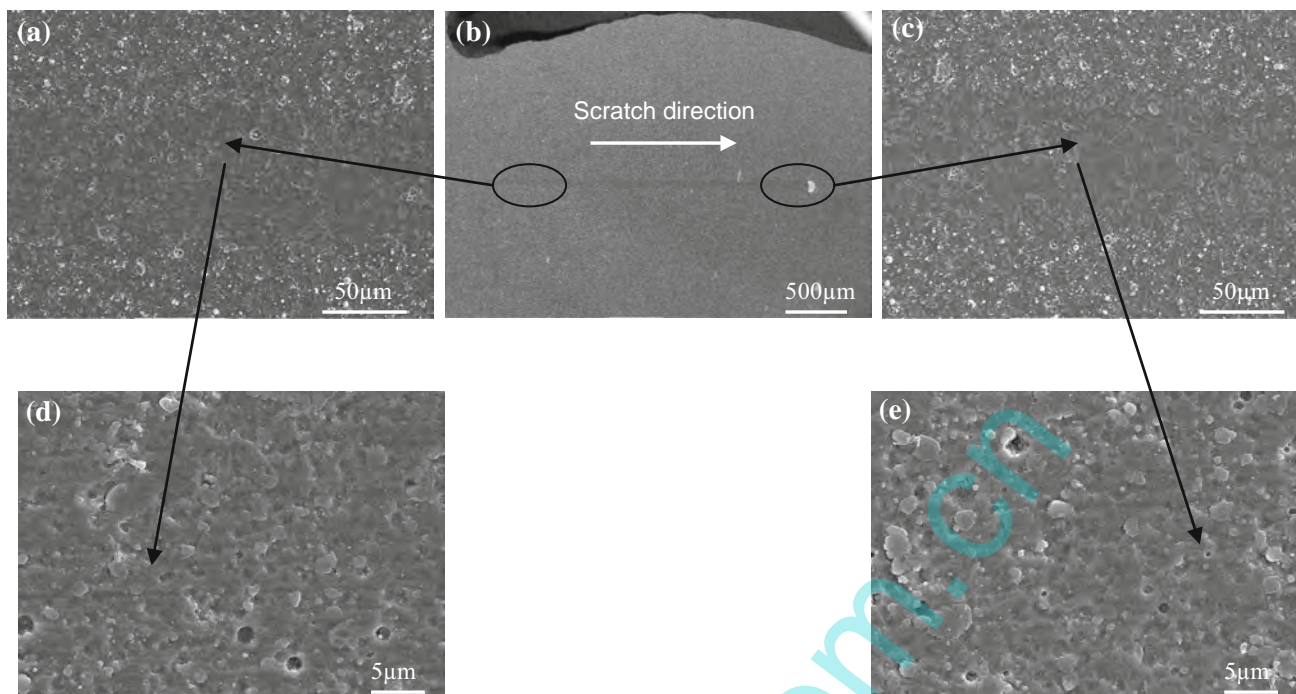
Fig. 7 Scratch morphologies of the AlTiN coating. **a** Scratch beginning, **b** whole morphology of the scratch, **c** scratch end, **d** high magnification morphology of the beginning, **e** high magnification morphology of the end
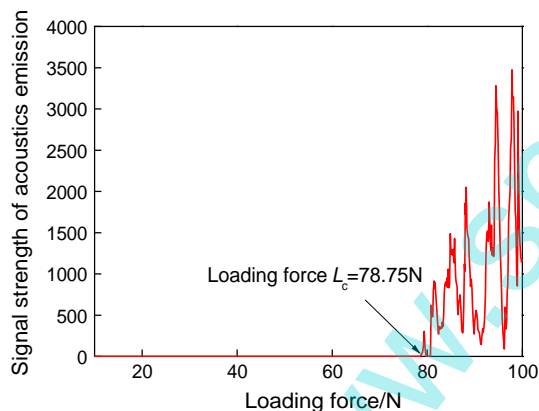

Fig. 8 Interfacial bonding strength

397.3 eV, and that of N–O key was 399 eV, which should be AlN phase because the binding energy of N element was 396.74 eV.

3.4 Line scan of the interface

After polishing treatment, the line scans of the coating interface were analyzed with FESEM configured EDS, and the line scans of the AlTiN binding interface were analyzed as shown in Fig. 6a–c. The elements of Al, Ti and N rose sharply at the coating–substrate interface, and a few were diffused into the substrate. The content of C atom was relatively stable due to the sample exposed to the air, showing that the C atoms

were not diffused into the substrate, as shown in Fig. 6d. Figure 6e shows that O atoms were stepped into the coating surface during the deposition, which was consistent with the analysis of valence state of O element by XPS. The source of O element shows as follows: (1) There were some O_2 in the deposition chamber, and Al^{3+} and Ti^{4+} were highly active metal ions, which were very easy to generate Al_2O_3 and TiO_2 with O_2 to deposit in the coating with other phases, which was benefited to improving wear resistance of the AlTiN coating. Figure 4 shows XRD analysis of AlTiN coating, there were not oxide phases Al_2O_3 and TiO_2, which explained that the mild oxidation was occurred on the coating surface. (2) The samples would adsorb O_2 in the air as cooling and exposing to the air, consequently, the presence of O_2 was inevitable. The atoms of W and Co cemented the substrate were negligible in the coating, as shown in Fig. 6f–g.

3.5 Interfacial bonding strength

Bonding strength of the AlTiN coating was measured with a WS-2005 type thin film adhesion strength scratch tester scratching tester, the measured parameter as follows: load of 100 N, loading rate of 50 N/min and scratch length of 6 mm, and the measured method was acoustic emission. Under the loading force of 100 N, the scratch morphologies were showed in Fig. 7, in which Fig. 7d, e was corresponded with high magnification morphology of the scratch beginning (Fig. 7a) and the scratch end (Fig. 7c),
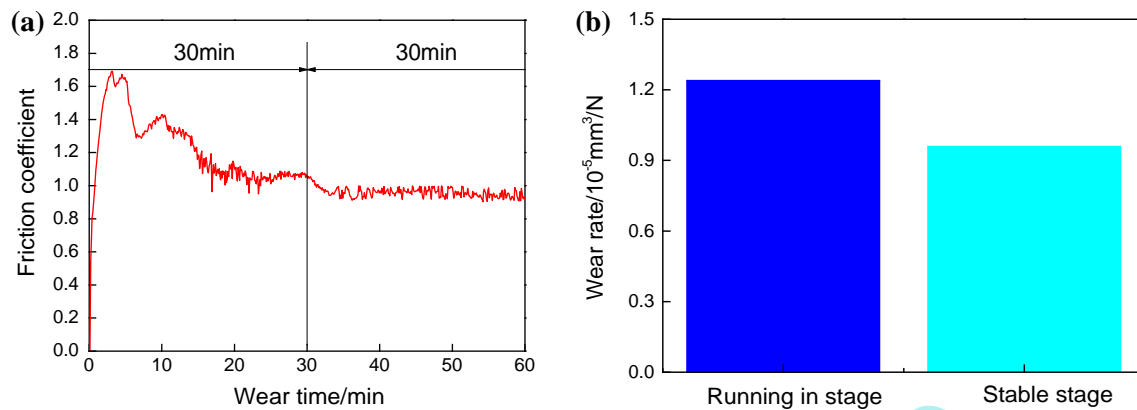
Fig. 9 Friction coefficients and abrasion rate. **a** Friction coefficients versus wear time, **b** abrasion rate
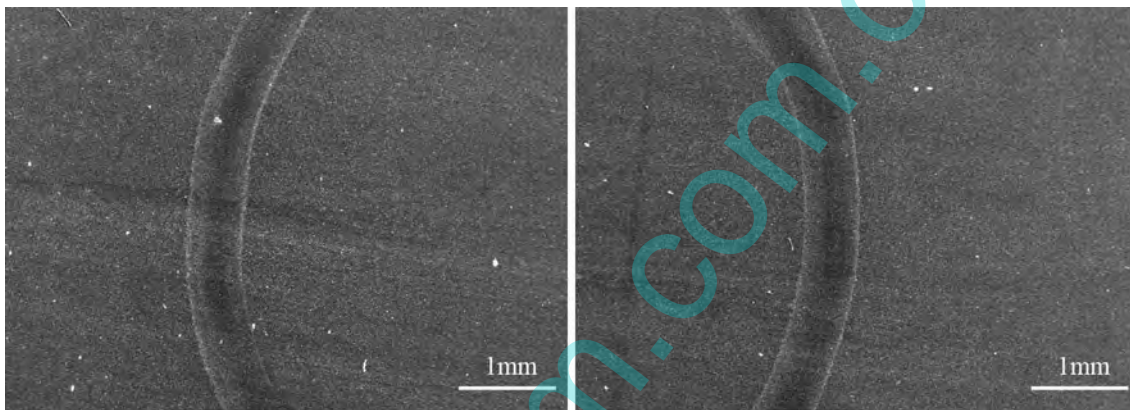

Fig. 10 Worn morphologies of AlTiN coating

respectively, the coating still maintained its integrity and no damages happened from the beginning to the end, indicating that the coating had a strong bonding strength with the substrate.

The continuous acoustic emission signals appeared at the load of 78.75 N, which was bonding strength of the AlTiN coating, shown as Fig. 8. Combining with scratch morphology in Fig. 7b, it can be inferred that the coating began to lacerate, and bonding strength of the AlTiN coating was the critical load of 78.75 N. Because the high energy ion bombarded and activated the atoms of the substrate surface, the coating had high bonding strength, which improved the coating compactness and mutual diffusion, and the replaced actions were occurred in the coating to form metallurgical bonding.

3.6 Friction and wear properties

Under the load of 5 N, the wear process of AlTiN coating at high temperature was divided into the running-in stage and stable stage, as shown in Fig. 9a. The average wear friction coefficient at high temperature of 800 °C for 1 h is 1.090, of which the first 30 min, the average friction coefficient was 1.2202, the average friction coefficient was 0.9591 in the late 30 min. The higher friction coefficient of AlTiN coating at the high temperature was due to the rough coating surface by cathode ion plating, the abrasion rate in the running-in stage was 1.24×10^{-5} m^3/N, while that in the stable stage was 0.96×10^{-5} m^3/N, shown in Fig. 9b, decreasing by 22.6 %, showing that AlTiN coating had excellent wear resistance.

In the condition of dry wear, the worn morphologies of AlTiN coating at high temperature of 800 °C were showed in Fig. 10, the worn scar width was about 600 μm. There were no surface defects and cracks after wear, but there were some obvious worn marks, which was due to the result of abrasive wear.

4 Conclusions

1. The elements of Al and N mainly exist in the AlTiN coating with AlN and AlTiN hard phase, and the Ti element mainly exists in the coating with TiN hard

phase, which is conducive to improving wear resistance of AlTiN coating.

2. The elements of Al, Ti and N are diffused at the coating interface, in which the part of Ti atoms are replaced by Al atoms at the TiN lattice, and still keep FCC structure of TiN coating to form metallurgical bonding, which is benefited to improving the coating–substrate bonding strength.

3. Bonding strength of the AlTiN coating–substrate measured by scratching tester is about 84.25 N, showing that AlTiN coating–substrate has good binding force.

References

1. J.L. Mo, M.H. Zhu, A. Leyland et al., Impact wear and abrasion resistance of CrN, AlCrN and AlTiN PVD coatings. Surf. Coat. Technol. **215**, 170–177 (2013)

2. E. Soroka, B. Lyashenko, S. Qiao et al., Tribological behaviour and cutting performance of PVD-TiN coating/substrate system with discontinuous surface architecture. Rare Metal Mater. Eng. **40**(4), 0580–0584 (2011)

3. Y. Fenga, L. Zhanga, R. Ke et al., Thermal stability and oxidation behavior of AlTiN, AlCrN and AlCrSiWN coatings. Int. J. Refract. Metals Hard Mater. **43**, 241–249 (2014)

4. L. Aihua, D. Jianxin, C. Haibing et al., Friction and wear properties of TiN, TiAlN, AlTiN and CrAlN PVD nitride coatings. Int. J. Refract. Metals Hard Mater. **31**, 82–88 (2012)

5. L. Zheng, Y. Wang, L. Zhao et al., Study on the fracture toughness of TiN/TiAlN coating. Rare Metals Mater. Eng. **37**(1), 752–755 (2008)

6. X. Chen, D. Yi, D. Huang et al., Thermal oxidation resistance of TiN/TiCN/A1$_2$0$_3$/TiN multilayer coatings on cemented carbide by chemical vapor deposition. Chin. J. Nonferrous Metals **21**(8), 1967–1973 (2011)

7. Y.Q. Wei, Li Chunwei, C. Gong et al., Microstructure and mechanical properties of TiN/TiAlN multilayer coatings deposited by arc ion plating with separate targets. Trans. Nonferrous Metals Soc. China **21**, 1068–1073 (2011)

8. Q.H. Luo, H.S. Yang, Y.H. Lu et al., Effect of AlTiN composition multilayer coatings periodic structure on adhesion. J. Aeronaut. Mater. **30**(2), 45–50 (2010)

9. W. Baoyun, L. Zhengxian, Y. Peng et al., Microstructures & performance of multilayer TiN/TiAlN coating on TC4 by arc ion plating. Rare Metal Mater. Eng. **37**(8), 1407–1410 (2008)

10. J. Bujak, J. Walkowicz, J. Kusinski, Influence of the nitrogen pressure on the structure and properties of (Ti, Al) N coatings deposited by cathodic vacuum arc PVD process. Surf. Coat. Technol. **180–181**, 150–157 (2004)

11. D. Kong, Y.H. Fu, Y.H. Wu et al., Surface and interface properties of TiN films grown by physical vapor deposition. J. Vac. Sci. Technol. **32**(12), 1078–1083 (2012)

12. R. Le Strydom, S. Hofmarm, The contribution of characteristic energy losses in the core-level X-ray photoelection spectroscopy peaks of TiN and (Ti, Al)N studied by electron energy loss spectroscopy and X-ray photoelectron spectroscopy. J. Electron Spectrosc. Relat. Phenomena **56**, 85–103 (1991)

13. H.C. Barshilia, K. Yogesh, K.S. Rajam, Deposition of TiAlN coatings using reactive bipolar-pulsed direct current unbalanced magnetron sputtering. Vacuum **83**, 427–434 (2009)